

## Differential Cross-Section of High-Mass Muon Pairs Produced by a 194 GeV/c $\pi^-$ Beam on a Tungsten Target

NA10 Collaboration

- B. Betev<sup>1a</sup>, J.J. Blaising<sup>4b</sup>, P. Bordalo<sup>3</sup>, A. Boumediene<sup>3</sup>, L. Cerrito<sup>3</sup>, A. Degré<sup>4b</sup>, A. Ereditato<sup>2</sup>,
- S. Falciano <sup>5</sup>c, K. Freudenreich<sup>1</sup>, E. Gorini<sup>2</sup>, M. Guanziroli<sup>5</sup>, H. Hofer<sup>5</sup>, P. Juillot<sup>4</sup>, L. Kluberg<sup>3</sup>,
- P. Lecomte<sup>5</sup>, P. Le Coultre<sup>5</sup>, R. Morand<sup>4b</sup>, B. Mours<sup>4b</sup>, A. Romana<sup>3</sup>, R. Salmeron<sup>3</sup>, P. Strolin<sup>2</sup>, H. Suter<sup>5</sup>, V.L. Telegdi<sup>5</sup>, J. Varela<sup>3d</sup>, G. Viertel<sup>5</sup>, J. Wallace-Hadrill<sup>1</sup>, M. Winter<sup>4</sup>
- <sup>1</sup> CERN, CH-1211, Geneva 23, Switzerland
- <sup>2</sup> University of Naples and INFN, I-80125 Naples, Italy
- <sup>3</sup> École polytechnique, F-91128 Palaiseau, France
- <sup>4</sup> CRN and University Louis Pasteur, F-67037 Strasbourg, France
- <sup>5</sup> ETH, CH-8093 Zürich, Switzerland

Received 16 January 1985

**Abstract.** We present a measurement of the production of muon pairs in 194 GeV/c  $\pi^-$ -tungsten interactions. A sample of 155,000 events with mass higher than 4.07 GeV/c<sup>2</sup> has been used to determine the differential cross-section as a function of the scaling variables  $\sqrt{\tau}$  and  $x_F$ .

Although many observed features of dilepton production by hadrons have been understood in terms of a "naïve" parton model [1] and QCD, there remain several open questions, namely the absolute magnitude of the cross-section and the effects of the anticipated scale-breaking. To study these important subjects, we are performing an experiment with greater statistics than previously available and with careful control of systematic errors.

In this Letter we report a measurement of the absolute cross-section for the production of massive muon pairs by  $194 \, \text{GeV/c} \, \pi^-$ 's on tungsten, based on a sample of 155,000 events with  $M \ge 4.07 \, \text{GeV/c}^2$  (M is the muon-pair mass). The dependence of the cross-section as a function of the scaling variables

 $\sqrt{\tau} = M/\sqrt{s}$  ( $\sqrt{s}$  is the total energy in the centre of mass) and Feynman  $x_F$  is studied.

The apparatus [2] has an acceptance covering a large domain in mass and rapidity, namely  $M \ge 2.4 \,\mathrm{GeV/c^2}$  and  $-0.15 \le y \le 0.9$ . A high luminosity was obtained by the use of a very intense beam [(1 to 2)×10<sup>9</sup>  $\pi^-$  per 2 s burst] on a heavy nuclear target (a 12 cm tungsten rod). The combination of large acceptance and high luminosity allows a differential analysis of events even more massive than the  $\Upsilon$ , a region heretofore unexplored with pion beams. Special emphasis was given to the determination of both the beam intensity and the chamber and trigger efficiencies so as to minimize systematic errors in the absolute value of the cross-section.

The experiment was carried out at the CERN Super Proton Synchrotron (SPS) with the spectrometer shown in Fig. 1. The unseparated  $\pi^-$  beam  $(95\,\%\,\pi^-,\,4.4\,\%\,\,K^-,\,0.6\,\%\,\bar{p})$  had a momentum bite of  $\pm\,10\,\%$  and an average intensity of  $1.3\times10^9\,\pi^-$  per burst. Beam that did not interact in the target was dumped into a tungsten and uranium plug 120 cm downstream from the target centre. This distance is large compared to the vertex resolution along the axis ( $\sigma\!<\!21\,\mathrm{cm}$ ) and thus the data are not contaminated by events from the beam dump. A carbon-iron absorber of  $13.4\,\lambda_{\mathrm{abs}}^\pi$ , starting 40 cm downstream from the target centre, surrounds the beam-dump plug. The spectrometer magnet is an air-core toroid with hexagonal symmetry which de-

<sup>&</sup>lt;sup>a</sup> Permanent address: Institute for Nuclear Research and Nuclear Energy, Sofia, Bulgaria

<sup>&</sup>lt;sup>b</sup> Now at LAPP, F-74019 Annecy-le-Vieux, France

<sup>°</sup> Now at INFN, Sezione di Roma, I-00100 Italy

<sup>&</sup>lt;sup>d</sup> Now at Centro de Fisica da Materia Condensada, Lisbon, Portugal

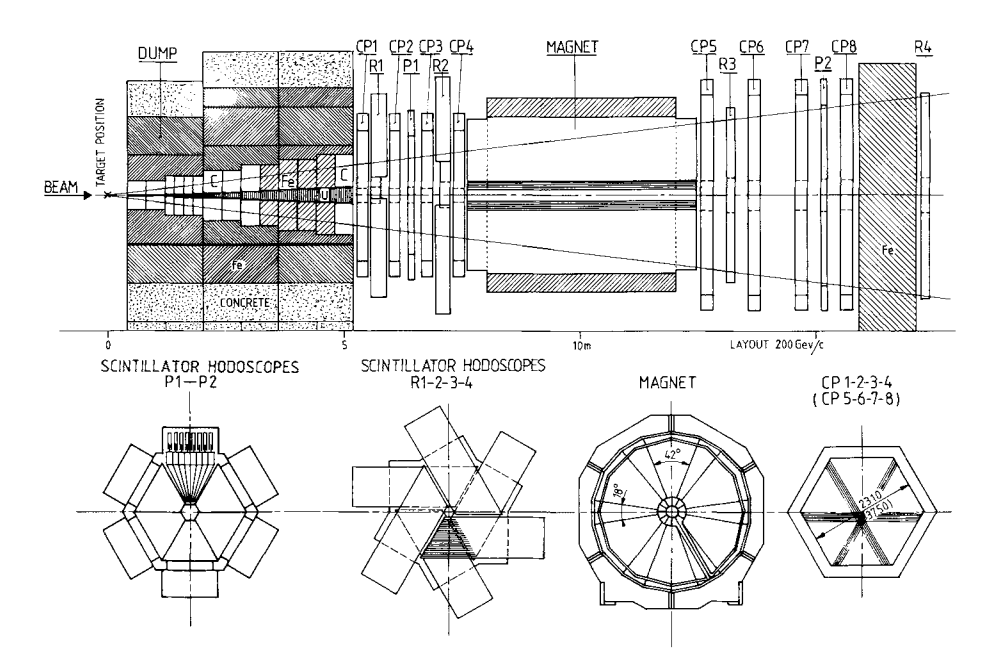


Fig. 1. Upper half: side view of the NA 10 spectrometer. Lower half: front view of the detectors and of the magnet

termines the geometrical structure of the multiwire proportional chambers CP and the scintillation counter hodoscopes R located upstream and downstream from the magnet. In this Letter, only data where both muons traversed the air sectors of the magnet are reported.

A fast first-level trigger requires the detection of at least one muon pointing to the target in at least two different sextants. Only muons with transverse momenta  $p_T$  above 800 MeV/c and pairs of mass greater than 2.4 GeV/c<sup>2</sup> are accepted by this first-level trigger. As these criteria are easily fulfilled by high multiplicity events, a second-level trigger, implemented with a microprocessor system [3], rejects events when the number of wires or counters which fire exceeds some preset value. The inefficiencies induced by this second-level trigger are continuously monitored by accepting a small subsample of flagged firstlevel triggers. The analysis of this subsample shows that these cuts result only in a loss of 0.5% of the events of the final sample under standard conditions  $(1.3 \times 10^9 \,\pi^- \text{ per burst})$ .

In the off-line processing, tracks are reconstructed for the downstream and upstream chamber telescopes. The segments found in these two telescopes have to be validated by the scintillation counters; this requirement removes time-accidental tracks. The momenta are determined with an iterative algorithm which uses a measured field map; the momentum accuracy is better than 2%, independent of  $p_T$ . Corrections for the energy losses in the hadron absorber and in the target are applied. A further selection of the tracks is made with a momentum-dependent algorithm which is based on the distance between and

the coplanarity of the upstream and downstream segments of a complete track candidate in the magnet midplane, and on the distance between the upstream segment and the beam axis at the target. These constraints reduce the number of like-sign events (which at this level are mostly random associations of tracks) by a factor of 7, whereas they result in a 1.5% loss of opposite-sign events. The vertex is determined from the two muon directions downstream from the absorber, taking into account the multiple scattering in the absorber, the muon momenta, and the finite size of the beam. The resulting mass resolution is 3% at  $M = 10 \, \text{GeV/c}^2$ .

The counter and trigger efficiencies were periodically determined in dedicated runs, during which special hodoscopes P1 and P2 (see Fig. 1) provide a trigger independent of the elements of the standard trigger. This combined counter and trigger efficiency is 96%. The overall reconstruction efficiency was determined from a special analysis of the data. Two per cent of the events were lost owing to chamber inefficiencies, and 1.5% owing to the reconstruction algorithm. These and the previous factors correspond for an intensity of  $1.3 \times 10^9 \, \pi^-$  per burst to an overall efficiency of  $(91 \pm 5)\%$ ; for the highest intensity available, i.e.  $2 \times 10^9 \, \pi^-$  per burst, this decreases to 83%.

As already pointed out, special attention was devoted to the measurement of the absolute beam intensity. Two ionization chambers filled with argon, located in the beam, measured the flux. Three independent scintillation-counter telescopes, perpendicular to the beam, monitored the targeting efficiency. The relative calibration of the ionization chambers

Table 1. The number of opposite-sign events, like-sign events, and acceptance as a function of M and  $x_F$ . The  $\Upsilon$  region is included. The acceptance (Acc.) in this region has been calculated in the same way as in the continuum region

M	XF	μ+μ-	μ+μ+,μ-μ-	Acc.
[GeV/c <sup>2</sup> ]				[%]
4.07-4.66	-0.1-0.0	2067	21	1.19
	0.0-0.1	10603	102	5.65
	0.1-0.2	16464	106	8.63
	0.2-0.3	13383	57	7.80
	0.3-0.4	6576	21	4.60
	0.4-0.5	1422	5	1.23
4.66-5.26	-0.1-0.0	1414	7	1.65
	0.0-0.1	6077	24	6.33
	0.1-0.2 0.2-0.3	9465 9088	28	10.07
	0.2-0.3	5437	16	10.04 6.91
	0.4-0.5	2122	4	3.20
5.26-5.85	-0.1-0.0	930	7	2.00
5.20-5.05	0.0-0.1	3394	9	2.00 6.24
	0.1-0.2	5675	12	10.30
	0.2-0.3	5879	5	11.03
	0.3-0.4	4164	i	8.51
	0.4-0.5	2149	1	5.15
	0.5-0.6	561	0	1.82
5.85-6.45	-0.1-0.0	690	1	2.62
	0.0-0.1	2070	2	6.61
	0.1-0.2	3452	3	10.28
	0.2-0.3	3879	2	11.95
	0.3-0.4	2942	0	10.36
	0.4-0.5 0.5-0.6	1764 710	0	6.73 3.73
		<del></del>		
6.45-7.06	-0.1-0.0 0.0-0.1	447 1264	1	2.93 6.88
	0.1-0.2	2099	2	10.57
	0.2-0.3	2509	2	12.24
	0.3-0.4	2134	0	11.20
	0.4-0.5	1355	0	8.35
	0.5-0.6	680	0	5.27
	0.6-0.7	204	1	2.37
7.06-7.68	-0.1-0.0	268	o	3.32
	0.0-0.1	758	0	6.77
	0.1-0.2	1283	0	10.78
	0.2-0.3	1620	0	12.83
	0.3-0.4 0.4-0.5	1436 1033	0	12.83 9.90
	0.5-0.6	522	0	7.16
	0.6-0.7	223	ő	4.24
	0.7-0.8	38	1	1.36
7.68-8.30	-0.1-0.0	175	0	4.0
	0.0-0.1	456	Ö	7.0
	0.1-0.2	808	o	10.1
	0.2-0.3	1006	0	13.3
	0.3-0.4	962	0	13.3
	0.4-0.5	752	0	11.6
	0.5-0.6 0.6-0.7	402	0	8.2
	0.7-0.8	190 38	0	5.2 2.8
8 20 9 02	0100		<del></del>	
8.30-8.93	-0.1-0.0	127	0	4.0
	0.0-0.1	306	0	7.3
	0.1-0.2 0.2-0.3	478 672	0	10.0
	0.2-0.3	659	0	12.2 14.3
	0.4-0.5	517	1	13.2
		, ,,,,		1 43.4
	0.5-0.6	306	0	9.6
		306 121	0	9.6 7.6

M [GeV/c²]	ХF	μ+μ-	μ+μ+,μ-μ-	Acc. [%]
8.93- 9.57	- 0.20.1 - 0.1- 0.0 0.0- 0.1 0.1- 0.2 0.2- 0.3 0.3- 0.4 0.4- 0.5 0.5- 0.6 0.6- 0.7 0.7- 0.8	17 106 249 452 596 584 473 243 112 28	0 0 0 0 0 0 0 0	1.0 4.3 7.0 9.4 13.2 14.5 13.7 10.8 6.7 8.1
9.57-10.22	- 0.2 0.1 - 0.1- 0.0 0.0- 0.1 0.1- 0.2 0.2- 0.3 0.3- 0.4 0.4- 0.5 0.5- 0.6 0.6- 0.7 0.7- 0.8	16 79 162 325 388 465 329 187 60 16	0 0 1 0 0 0 0 0	1.3 3.9 6.8 8.2 11.4 13.8 11.9 9.9 8.0 12.0
10.22-10.88	-0.20.1 -0.1- 0.0 0.0- 0.1 0.1- 0.2 0.2- 0.3 0.3- 0.4 0.4- 0.5 0.5- 0.6 0.6- 0.7	9 40 93 123 200 201 190 113 45	0 0 2 0 0 0 0	1.7 3.9 6.6 8.7 10.2 12.5 12.3 11.5 7.1
10.88-12.25	-0.20.1 -0.1- 0.0 0.0- 0.1 0.1- 0.2 0.2- 0.3 0.3- 0.4 0.4- 0.5 0.5- 0.6 0.6- 0.7	8 21 43 86 132 157 143 77 31	0 0 0 0 0 0 0	3 ,5 7 10 11 12 11 11 9
12.25-13.68	-0.20.1 -0.1- 0.0 0.0- 0.1 0.1- 0.2 0.2- 0.3 0.3- 0.4 0.4- 0.5 0.5- 0.6	2 5 11 21 36 35 22 14	0 0 0 0 0 0	1 7 10 9 10 11 9
13.68-15.19	-0.1- 0.0 0.0- 0.1 0.1- 0.2 0.2- 0.3 0.3- 0.4 0.4- 0.5 0.5- 0.6	2 2 5 3 4 1	0 0 0 0 0 0	5 3 8 5 9 4

<b>Table 2.</b> The cross-section $d^2 \sigma/d \sqrt{\tau} dx_F$ integrated ove	r each $\sqrt{\tau} - x_F$ cell as a	a function of $\sqrt{\tau}$ and $x_F$ . The Y
region has been excluded. The integrated luminosity is		

$\sqrt{\tau}$	$x_F$	d²σ/d√τdx <sub>F</sub> [nb/nucleus]
0.21-0.24	-0.1-0.0	$(2.03 \pm 0.08)$
ĺ	0.0-0.1	$(2.19 \pm 0.03)$
	0.1-0.2	$(2.22 \pm 0.02)$
	0.2-0.3	$(2.00 \pm 0.02)$
ì	0.3-0.4	$(1.66 \pm 0.03)$
}	0.4-0.5	$(1.34 \pm 0.05)$
0.24-0.27	- 0.1-0.0	$(1.00 \pm 0.04)$
İ	0.0-0.1	$1.12 \pm 0.02$
	0.1-0.2	$1.09 \pm 0.02$
	0.2-0.3	$1.05 \pm 0.01$
	0.3-0.4	$0.92 \pm 0.02$
	0.4-0.5	$0.75 \pm 0.02$
0.27-0.30	- 0.1-0.0	$(0.54 \pm 0.02)$
1	0.0-0.1	$0.63 \pm 0.01$
	0.1-0.2	$0.64 \pm 0.01$
	0.2-0.3	$0.62 \pm 0.01$
	0.3-0.4	$0.57 \pm 0.01$
	0.4-0.5	$0.49 \pm 0.01$
	0.5-0.6	$0.36 \pm 0.02$
0.30-0.33	-0.1-0.0	$(0.31 \pm 0.01)$
i	0.0-0.1	$0.36 \pm 0.01$
	0.1-0.2	$0.39 \pm 0.01$
ĺ	0.2-0.3	$0.38 \pm 0.01$
[	0.3-0.4	$0.33 \pm 0.01$
	0.4-0.5	$0.31 \pm 0.01$
	0.5-0.6	$0.22 \pm 0.01$
0.33-0.36	-0.1-0.0	$(0.178 \pm 0.010)$
	0.0-0.1	$0.214 \pm 0.008$
	0.1-0.2	$0.231 \pm 0.007$
	0.2-0.3	$0.239 \pm 0.007$
ł	0.3-0.4	$0.222 \pm 0.007$
ĺ	0.4-0.5	$0.189 \pm 0.007$
1	0.5-0.6	$0.150 \pm 0.007$
	0.6-0.7	$0.100 \pm 0.009$

$\sqrt{\tau}$	XF	$d^2\sigma/d\sqrt{\tau}dx_F$
		[nb/nucleus]
0.36-0.39	~ 0.1- 0.0	$(0.094 \pm 0.007)$
	0.0- 0.1	$0.130 \pm 0.006$
	0.1- 0.2	$0.139 \pm 0.005$
	0.2- 0.3	$0.147 \pm 0.005$
1	0.3- 0.4	$0.130 \pm 0.005$
	0.4- 0.5	$0.121 \pm 0.005$
	0.5- 0.6	$0.085 \pm 0.005$
}	0.6~ 0.7	$0.061 \pm 0.005$
	0.7~ 0.8	$0.033 \pm 0.007$
0.39-0.42	-0.1- 0.0	(0.051 ± 0.005)
	0.0- 0.1	$0.076 \pm 0.005$
	0.1- 0.2	$0.093 \pm 0.004$
	0.2- 0.3	$0.088 \pm 0.004$
	0.3- 0.4	$0.084 \pm 0.004$
	0.4- 0.5	$0.075 \pm 0.004$
	0.5- 0.6	$0.057 \pm 0.004$
	0.6- 0.7	$0.042 \pm 0.004$
	0.7- 0.8	$0.016 \pm 0.003$
0.54-0.60	- 0.2 0.1	$(0.0033 \pm 0.0017)$
	~ 0.1~ 0.0	$(0.0053 \pm 0.0014)$
	0.0- 0.1	$0.0071 \pm 0.0014$
	0.1- 0.2	$0.0105 \pm 0.0015$
	0.2- 0.3	$0.0142 \pm 0.0017$
}	0.3- 0.4	$0.0156 \pm 0.0017$
	0.4- 0.5	$0.0156 \pm 0.0018$
	0.5- 0.6	$0.0084 \pm 0.0013$
	0.6- 0.7	$0.0041 \pm 0.0011$
0.60-0.66	-0.20.1	$(0.0019 \pm 0.0019)$
j	-0.1- 0.0	$(0.0009 \pm 0.0008)$
	0.0- 0.1	$0.0013 \pm 0.0006$
	0.1- 0.2	$0.0028 \pm 0.0008$
	0.2- 0.3	$0.0042 \pm 0.0010$
	0.3- 0.4	$0.0038 \pm 0.0009$
	0.4- 0.5	$0.0028 \pm 0.0009$
	0.5- 0.6	$0.0017 \pm 0.0006$
0.66-0.72	-0.1- 0.0	$(0.0004 \pm 0.0004)$
	0.0~ 0.1	$0.0009 \pm 0.0009$
	0.1- 0.2	$0.0008 \pm 0.0007$
	0.2- 0.3	$0.0007 \pm 0.0006$
	0.3- 0.4	$0.0005 \pm 0.0005$
	0.4- 0.5	$0.0003 \pm 0.0003$

was performed periodically by activating carbon foils at the running intensity\*. The  $^{11}$ C decay rate was determined with a NaI detector calibrated to  $\pm 2.5$ %. The absolute calibration was obtained in two ways:

- a) at low flux  $(10^6 \text{ to } 10^7/\text{s})$  by measuring the beam intensity directly with scintillation counters;
- b) at the running flux by activating carbon foils with 400 GeV protons (using the known  $p-{}^{11}\text{C}$  cross-section [4]).

The two methods agreed well, yielding a beam calibration accurate to  $\pm 4\%$ .

The beam spot was monitored at the target with a wire chamber with current integration readout.

The actual spot size was determined by the activation of 1 mm wide carbon foils and yielded a FWHM of 0.5 cm. The target diameter is 1.8 cm so that the survey of the beam position with the beam wire chamber ensures full targeting efficiency.

Within the spectrometer acceptance,  $J/\psi$ 's are about twenty times more abundant than events with  $M>4.07~{\rm GeV/c^2}$ . The overall efficiency and the running conditions could therefore be continuously monitored through the absolute  $J/\psi$  yield both on-line and off-line

The smearing function, which correlates the true value of the variables with the measured one, and the acceptance in the variables  $\sqrt{\tau}$  and  $x_F$  were determined with a Monte Carlo simulation program and the same reconstruction program as used for the data. The dimuons were generated with:

<sup>\*</sup> V. Agoritsas, A. Müller and A. Regelbrügge are warmly thanked for their special assistance in these measurements

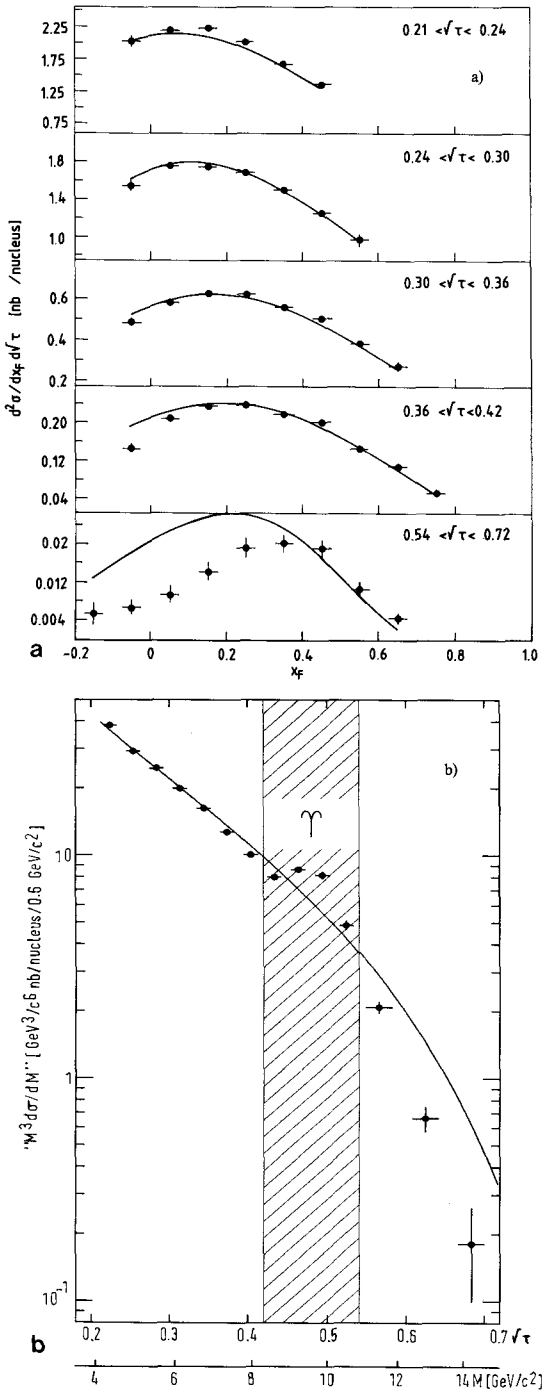


Fig. 2. a Plot of  $d^2 \sigma/d \sqrt{\tau} \, dx_F$  for five intervals in  $\sqrt{\tau}$ . The parameters of the valence pion structure function and the absolute normalization were fitted to the data using the Drell-Yan formalism and the structure function parameters of the nucleon and the pion sea of [13]. The fitted parameters were  $\alpha_\pi = 0.40 \pm 0.02$ ,  $\beta_\pi = 1.17 \pm 0.03$ , and  $\langle K \rangle = 2.49 \pm 0.06$ . The full line represents the predictions of the "naïve" Drell-Yan model multiplied by 2.49. b Plot of  $M^3 \, d\sigma/dM$  integrated between  $0 \le x_F \le 0.5$  as a function of  $\sqrt{\tau}$  and M. The mean  $\sqrt{s}$  of the data is equal to 19.1 GeV. The partial nature of this cross-section is emphasized by the quotation marks in the figure. The full line represents, as in a, the "naïve" Drell-Yan model multiplied by 2.49

- a) a uniform distribution in  $\phi$ , the azimuthal decay angle;
- b) a  $1 + \lambda \cos^2 \theta$  distribution in the centre of mass of the dimuon with  $\lambda = 1$ , where  $\theta$  is defined in the Collins-Soper frame [5];
- c) a dimuon transverse momentum  $(P_T)$  distribution as given in [6];
- d) a generating function  $f(\sqrt{\tau}, x_F)$ , which is essentially the Drell-Yan cross-section using the Buras-Gaemers [7] parametrization of the structure functions.

The measured momentum and spatial distributions of the  $\pi^-$  beam were allowed for. The Fermi motion, the dominant term in the smearing function, was taken into account following [8], but cut at 0.4 GeV/c. This smearing in s, the acceptance in s, and the s dependence of the production, when convoluted, induce a distortion in the  $\sqrt{\tau}$  (or mass) spectrum (with respect to the spectrum corresponding to a sharp s). The distortion may be illustrated by the relation  $\sqrt{\tau} = M/\sqrt{s(M)}$ , with  $\sqrt{s(M)} = 19.4$   $-0.04 \times M + 0.01 \times M^2$ . This particular relation is obtained from Monte Carlo studies. Similar effects in  $x_F$  occur but are less important. Full details of the analysis can be found in [9].

The Monte Carlo sample consists of 10<sup>6</sup> accepted events satisfying the same trigger requirements and selection criteria as the data. We verified that the simulated distributions agreed globally with the observed ones for the three variables  $\phi$ ,  $\theta$ , and  $P_T$ which were integrated over for the calculation of the two-dimensional acceptance in  $\sqrt{\tau}$  and  $x_F$ . Because the acceptances in  $P_T$  and  $\phi$  are essentially flat, the integration over these variables is rather insensitive to the assumed distributions. A preliminary investigation [10] of the angular distributions indicates that  $\lambda$  differs from 1 only for  $M < 7 \,\mathrm{GeV/c^2}$  and  $x_1 > 0.6$  ( $x_1 =$  fractional antiquark momentum in the pion). Since this class of events represents only 4% of the total, the impact on the acceptance is negligible.

The present measurement is based on 155,000 opposite-sign dimuon events with  $M \ge 4.07 \,\mathrm{GeV/c^2}$ , which satisfy the selection criteria described above. About two thirds of the data were obtained with a 12 cm long W target, and one third with a shorter target (5.6 cm); their comparison shows no appreciable secondary interaction effects for  $x_F > 0$ . Background may be evaluated from the 444 like-sign events. The latter may be attributed to: i) heavy flavour production, ii) random association of two uncorrelated muons, iii) pion "punch-through", or iv) multiple pion production with subsequent decay of two pions to muons. Under the extreme assumption

that all like-sign events were due to heavy flavour production and that their corresponding opposite-sign contribution was ten times greater [11], the resulting contamination would be less than 6% in the worst region, i.e.  $M \le 4.7 \text{ GeV/c}^2$ ; however, a simple estimate indicates that all our like-sign events can be explained in terms of (iv).

The number of opposite-sign dimuons, the number of like-sign dimuons, and the acceptance with the effect of smearing folded in are displayed in Table 1 as a function of M and  $x_F$ . For  $M > 10.9 \text{ GeV/c}^2$  there are 852 events, without any like-sign background.

The cross-section is obtained from the observed distribution of events by deconvolution, i.e. by varying the parameters of the function  $f(\sqrt{\tau}, x_F)$  iteratively until the data are reproduced. Only those cells are considered where the acceptance is greater than 1%. The absolute normalization is obtained with the luminosities and overall efficiencies corresponding to each run. In Table 2 the cross-section  $d^2 \sigma / d \sqrt{\tau} dx_F$  in nanobarns/W nucleus at  $\sqrt{s}$ =19.1 GeV is presented as a function of the variables  $\sqrt{\tau}$  and  $x_F$ . The quoted errors are statistical only, and no backgrounds have been subtracted. Our systematic errors are dominated by the uncertainties in the flux ( $\pm 4\%$ ), in the efficiencies ( $\pm 5\%$ ), and in the absorption cross-section for W [12]. Because of possible background contamination, the uncertainties in the differential cross-section for  $\sqrt{\tau}$  < 0.24 are comparable to, or even larger than, the statistical errors. In view of possible reinteraction effects, the same holds for the points with  $x_F < 0$ . For these reasons, the corresponding cross-sections are given in parentheses in Table 2.

Figure 2a shows the differential cross-section  $d^2 \sigma/d\sqrt{\tau} dx_F$  for five  $\sqrt{\tau}$  intervals. The predictions

of the "naïve" Drell-Yan model are also shown in Fig. 2a. A detailed comparison of the data with theory is reserved for the following Letter.

Figure 2b displays the cross-section " $M^3 d\sigma/dM$ " integrated between  $0 \le x_F \le 0.5$  as a function of  $\sqrt{\tau}$  and also as a function of M. The predictions of the "naïve" Drell-Yan model are again indicated (full line).

Acknowledgements. We should like to thank the members of the SPS operating crew and the Experimental Area group for the skilful operation of the beam line. We should like to express our gratitude to the engineering and technical staff of our Collaboration for their important contributions to the construction and operation of our apparatus. We gratefully acknowledge the contributions of D. Jensen in the last stage of the analysis. Finally we would like to thank M. Jouhet for preparing the manuscript.

## References

- S.D. Drell, T.M. Yan: Phys. Rev. Lett. 25, 316 (1970); Ann. Phys. (NY) 66, 578 (1971)
- 2. L. Anderson et al.: Nucl. Instrum. Methods 223 A, 26 (1984)
- J. Lecoq: Thèse de doctorat d'État, Université de Haute Alsace, Mulhouse, 1982, CRN/HE83-01 (unpublished); J. Lecoq et al.: Nucl. Instrum. Methods 213, 329 (1983)
- 4. S.B. Kaufmann et al.: Phys. Rev. C 13, 253 (1976)
- 5. J.C. Collins, D.E. Soper: Phys. Rev. **D** 16, 2219 (1977)
- O. Callot: Thèse de doctorat d'État, Orsay, Report LAL 81/05, 1981 (unpublished)
- 7. A.J. Buras, K.J.F. Gaemers: Nucl. Phys. B 132, 249 (1978)
- 8. A. Bodek, J.L. Ritchie: Phys. Rev. D 23, 1070 (1981)
- B. Mours: Thèse de 3<sup>eme</sup> cycle, Université Louis Pasteur, Strasbourg, 1984, CRN/HE84-06 (unpublished); J. Varela: Thèse de doctorat d'État, Université de Paris-Sud, Centre d'Orsay, 1984 (unpublished)
- B. Betev et al.: Contribution to the 22nd International Conference on High-Energy Physics, Leipzig, 1984
- H.G. Fischer, W.M. Geist: Z. Phys. C Particles and Fields 19, 159 (1983)
- 12. A.S. Carroll et al.: Phys. Lett. 80 B, 319 (1979)
- J. Badier et al.: Z. Phys. C Particles and Fields 18, 281 (1983)